CORROSION SCIENCE AND TECHNOLOGY, Vol.17, No.2(2018), pp.45~53 pISSN: 1598-6462 / eISSN: 2288-6524
[Research Paper] DOI: https://doi.org/10.14773/cst.2018.17.2.45

Surface Protection Obtained by Anodic Oxidation of New Ti-Ta-Zr Alloy

C. Vasilescu†, S. I. Drob, J. M. Calderon Moreno, P. Drob, M. Popa, and E. Vasilescu
Institute of Physical Chemistry Ilie Murgulescu of Romanian Academy, Bucharest, Romania
(Received December 18, 2017; Revised February 28, 2018; Accepted March 02, 2018)

A new 80Ti-15Ta-5Zr wt% alloy surface was protected by anodic oxidation in phosphoric acid solution. The protective oxide layer (TiO_2, ZrO_2 and Ta suboxides and thickness of 15.5 nm) incorporated PO_4^{3-} ions from the solution, according to high resolution XPS spectra. The AFM analysis determined a high roughness with SEM detected pores (20 - 50 nm). The electrochemical studies of bare and anodically oxidized Ti-15Ta-5Zr alloy in Carter-Brugirard saliva of different pH values and saliva with 0.05M NaF, pointed to a nobler surface for the protected alloy, with a thicker electrodeposited oxide layer acting as a barrier against aggressive ions. The oxidized alloy significantly decreased corrosion current densities and total quantity of ions released into the oral environment in comparison with the bare one, at higher polarisation resistance and protective capacity of the electrodeposited layer. The impedance data revealed a bi-layered oxidation film formed by: a dense, compact, barrier layer in contact with the metallic substrate, decreasing the potential gradient across the metal/oxide layer/solution interface, reducing the anodic dissolution and a more permissive, porous layer in contact with the electrolyte. The open circuit potential for protected alloy shifted to nobler values, with thickening of the oxidation film signifying long-term protection.

Keywords: *Ti-15Ta-5Zr alloy, Carter-brugirard saliva, Electrochemical behaviour, AFM, SEM*

1. Introduction

In the last years there are many researches for the development of new titanium alloys for biomedical applications that contain non-toxic and non-allergenic alloying elements [1-4]. The design and selection of new alloys depend on the intended medical application. These new metallic biomaterials must possess the following attributes: suitable mechanical properties (excellent combination of high strength and low modulus value, close to bone); biocompatibility (highly non toxicity that should not cause any inflammatory or allergic reactions in the human body); high corrosion and wear resistance, that is of prime importance for the longevity of the material in the human system; osseointegration (ability to integrate with the adjacent bone and other tissues) [5].

Titanium alloys show the greatest biocompatibility and corrosion resistance among metallic materials used as biomaterials. However, they are bioinert materials and sometimes present a tendency to corrode which is influenced by the aggressivity of physiological media. Therefore a surface treatment is necessary in order to achieve superior biocompatibility and corrosion resistance. There are many studies concerning various coatings for improved wear and corrosion resistance [6-8] and others regarding coatings for high osseointegration [9-11], but it is necessary to develop coatings that possess both properties. Li *et al.* [12] developed a new methodology to achieve these properties on a highly oxidized material: the alloy (Ti-Nb-Ta-Zr) was initially heat treated, later alkali treated and then immersed for 2 – 4 weeks in protein free body fluid (biomimetic solution). This two-step treatment, growths the surface oxide and enhances the formation of Ca–P compounds onto the surface. This method seems to be very promising because it increases the corrosion and wear resistance by forming TiO_2, ZrO_2 and Nb_2O_2 layers on the alloy's surface and also promotes the bioconductivity by the alkali treatment.

In this paper the surface of new Ti-15Ta-5Zr alloy [13] was protected by anodic oxidation in phosphoric acid solution. The resulting oxide layer was characterised regarding composition and thickness, surface topography and roughness, morphology and porosity; electrochemical and corrosion behaviour of new alloy with oxide layer was monitored by electrochemical techniques.

† Corresponding author: cora_vasilescu@yahoo.com

2. Experimental Procedure

2.1 Anodic oxidation of new Ti-15Ta-5Zr alloy surface

Electrodes in the shape of discs cut from as-cast new Ti-15Ta-5Zr alloy were used as substrates. Before oxidation, the electrode surface was ground with metallographic paper to assure a mirror surface and then the electrodes were ultrasonically degreased in acetone and ultrasonically washed in distilled water.

A 1M orthophosphoric acid (H_3PO_4) solution was used as oxidation electrolyte. The anodic oxidation process was developed at a current density of 10 μA for 30 min. The current density was kept constant with a high power current source (Matrix, China).

2.2 Composition and thickness of the oxide layer

The composition and thickness of the oxidation layer were determined by X-ray photoelectron spectroscopy (XPS). Quantera SXM equipment with a base pressure in the analysis chamber of 10^{-9} Torr was used. The X-ray source was Al K_α radiation (1486.6eV, monochromatized).

2.3 Topography and roughness of the oxide layer

The surface topography and roughness of the protected alloy surface were examined with an atomic force microscope type XE-100, (Park System, Korea) in non-contact mode; 2D and 3D topographic images were realised on a surface of 2 x 2 μm, The root mean square (RMS) and average (Rav) roughness were calculated.

2.4 Morphology and porosity of the oxide layer

The morphology and porosity of the oxidation film were studied by scanning electron microscopy (SEM) using a Quanta 3D FEG (FEI, Eindhoven, The Netherlands) equipment operating at 5 kV.

2.5 Electrochemical characterisation of oxide layer

Electrochemical characterisation of oxide layer was performed by cyclic potentiodynamic and linear polarisation, electrochemical impedance spectroscopy (EIS) and time monitoring of the open circuit potentials and corresponding potential gradients. All measurements were carried out in artificial Carter-Brugirard saliva of composition (g/L): NaCl – 0.7; KH_2PO_4 – 0.26; KSCN – 0.33; Na_2HPO_4 – 0.19; $NaHCO_3$ – 1.5; urea – 0.13. Saliva of different pH values (3.51; 7.62; 9.06) were used for simulating the real functional conditions in the oral cavity; after a meal, the pH becomes acidic [14,15] and during inflammations or infections alkaline [16]. Also, the case of using tooth pastes with fluorine was reproduced by adding 0.05M NaF to neutral saliva; this saliva has a pH value 7.94.

Voltalab 80 equipment and its VoltaMaster 4 program were used for the potentiodynamic polarisation and EIS techniques and a high performance Hewlett-Packard multimeter for potentials monitoring.

Cyclic potentiodynamic polarisation curves were registered with a scan rate of 1 mv/s starting at - 600 mV up to + 2000 mV (vs. SCE) and linear polarisation curves with the same scan rate for ±50 mV around the open circuit potential value. The main electrochemical and corrosion parameters were determined: corrosion potential (E_{corr}); passivation potential (E_p); tendency to passivation ($|E_{corr} - E_p|$); passive potential range (ΔE_p); passive current density (i_p); corrosion current density (i_{corr}); corrosion rate (V_{corr}); polarisation resistance (R_p); the total quantity of ions released into solution [17-19].

Nyquist and Bode EIS spectra were determined at the open circuit potential with 5 mV voltage amplitude in the frequency range from 10^{-1} Hz to 10^5 Hz. An electric equivalent circuit was modelled with ZView program.

The open circuit potentials (E_{oc}) were monitored for 1000 immersion hours in Carter-Brugirard saliva of different pH values and with added 0.05M NaF.

The open circuit potential gradients, due to the non-uniformities of the saliva pH, $\Delta E_{oc}(pH)$ and content, $\Delta E_{oc}(c)$ which could appear along the implant surface in oral cavity were calculated as:

$$\Delta E_{oc1}(pH) = E_{oc}^{pH=3.51} - E_{oc}^{pH=7.62} \quad (1)$$

$$\Delta E_{oc2}(pH) = E_{oc}^{pH=3.51} - E_{oc}^{pH=9.06} \quad (2)$$

$$\Delta E_{oc3}(pH) = E_{oc}^{pH=7.62} - E_{oc}^{pH=9.06} \quad (3)$$

$$\Delta E_{oc4}(c) = E_{oc}^{pH=7.62} - E_{oc}^{NaFpH=7.94} \quad (4)$$

3. Results and Discussion

3.1 Composition and thickness of the oxide layer

XPS analysis identified the constituent elements of Ti-15Ta-5Zr alloy and, in addition, O and P. Therefore, through the anodic oxidation, the surface of the Ti-15Ta-5Zr alloy was covered with an oxide layer formed by TiO_2, ZrO_2, Ta sub-oxides and PO_4^{3-} ions, incorporated in the time of the oxidation process from the H_3PO_4 solution. The presence of PO_4^{3-} ions will favour the ulterior co-deposition of phosphate ions from the physiological fluid, which will promote bone formation, i.e. conducts to bioactivity increase.

The oxide layer has a thickness of 15.5 nm [13] calculated from XPS depth profiling spectra in comparison with native oxide layer that has 8.5 ± 1 nm [20].

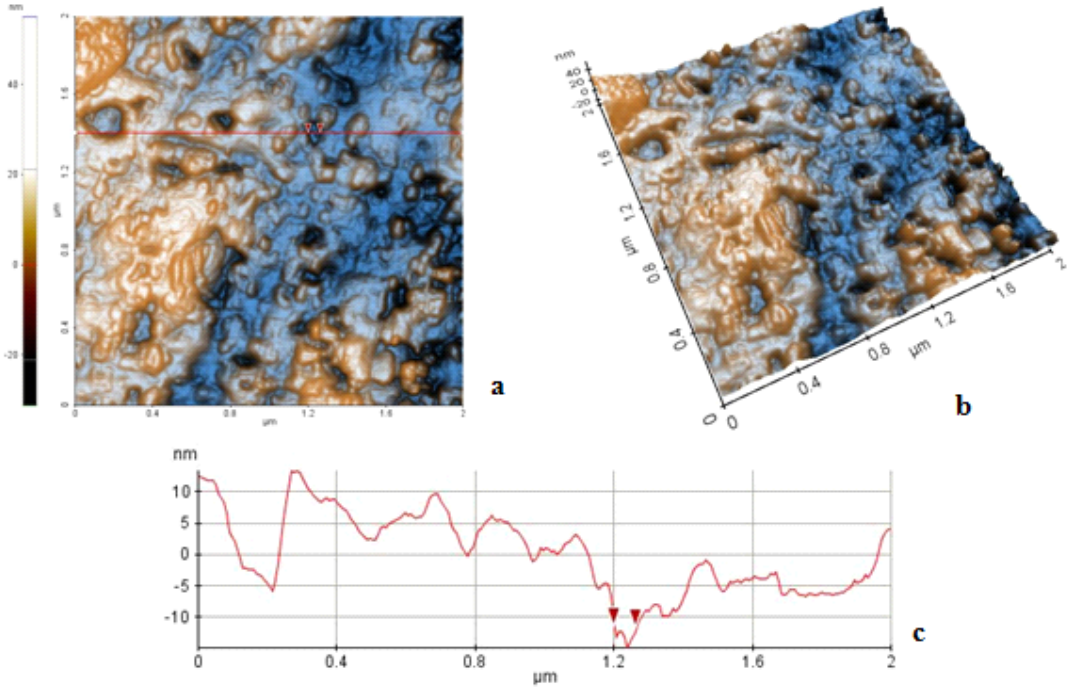

Fig. 1 AFM 2D (a) and 3D (b) images and line profile (c) for Ti-15Ta-5Zr alloy surface after anodic oxidation.

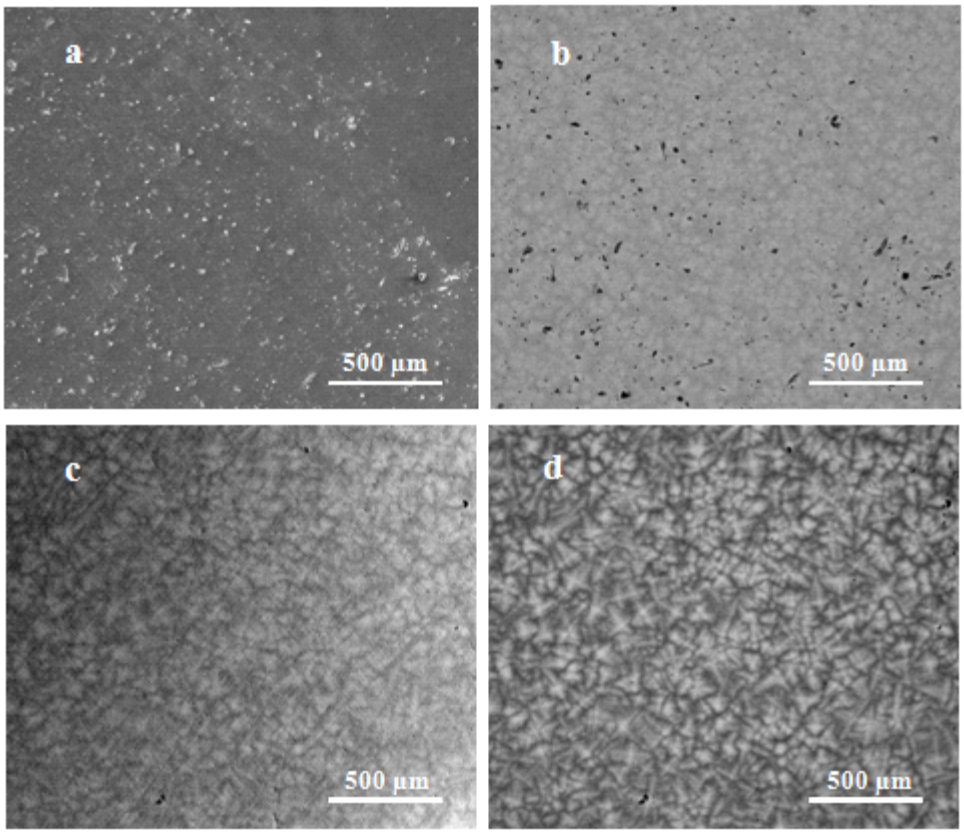

Fig. 2 SEM (a) and BSE (b) micrographs for Ti-15Ta-5Zr alloy surface after anodic oxidation; SEM (c) and BSE (d) micrographs for bare Ti-15Ta-5Zr alloy surface.

Table 1 Main electrochemical parameters for bare and anodic oxidation Ti-15Ta-5Zr alloy in Carter-Brugirard saliva, at 37 °C

Ti-15Zr-5Nb	E_{corr} (mV)	E_p (mV)	ΔE_p (mV)	$\lvert E_{corr} - E_p \rvert$ (mV)	i_p ($\mu A/cm^2$)
Saliva pH = 3.51					
Bare	-250	-100	>2000	150	0.5
Anodic oxidation	-200	-130	>2000	70	0.4
Saliva pH = 7.62					
Bare	-100	0	>2000	100	0.4
Anodic oxidation	-40	-10	>2000	30	0.23
Saliva pH = 9.06					
Bare	-300	-200	>2000	100	1.05
Anodic oxidation	-230	-210	>2000	20	0.8
0.05M NaF Saliva pH = 7.94					
Bare	-300	-150	>2000	150	1.2
Anodic oxidation	-250	-160	>2000	90	0.9

Table 2 Main corrosion parameters for bare and anodic oxidation Ti-15Ta-5Zr alloy in Carter-Brugirard saliva, at 37 °C

Ti-15Zr-5Nb	i_{corr} ($\mu A/cm^2$)	V_{corr} ($\mu m/yr$)	Resistance class	Ion release (ng/cm^2)	$R_{p\ (k\Omega.cm^2)}$
Saliva pH = 3.51					
Bare	0.028	0.259	Perfect Stable	26.31	1548.1
Anodic oxidation	0.009	0.083	Perfect Stable	8.43	1720.3
Saliva pH = 7.62					
Bare	0.0079	0.0645	Perfect Stable	6.55	2035.2
Anodic oxidation	0.0012	0.0098	Perfect Stable	0.99	3154.4
Saliva pH = 9.06					
Bare	0.025	0.231	Perfect Stable	23.47	1631.5
Anodic oxidation	0.005	0.046	Perfect Stable	4.67	1987.2
0.05M NaF Saliva pH = 7.94					
Bare	0.035	0.324	Perfect Stable	32.92	1028.9
Anodic oxidation	0.012	0.111	Perfect Stable	11.27	2112.8

3.2 Topography and roughness of the oxide layer

AFM images of the new alloy's surface after anodic oxidation (Fig. 1) show the surface topography and surface roughness of the oxide layer, indicating typical surface features with dimensions in the sub-micrometric and nanometric ranges, proper for the bone cell adhesion and proliferation. Root mean square (RMS) and average (Rav) surface roughness obtained from AFM measurements have values of 30.25 nm and respectively 26.52 nm, proving a good roughness, favourable for the deposition of new layers.

3.3 Morphology and porosity of the oxide layer

SEM microstructural studies of the alloy's surface after anodic oxidation in SE and BSE modes (Fig.s 2a and 2b) reveal the thickening of the passivating oxide layer present on the surface of the bare alloy, as shown by the disappearance of the signal from the subsurface alloy and the associated contrast caused by the different domains in the alloy's structure, due to the limited penetration depth of the electron beam. The alloy's subsurface domain structure is no longer visible in SE mode images (Fig. 2a), and clearly masked, barely distinguishable in BSE mode images (Fig. 2b), while is clearly visible in SE (Fig. 2c) and BSE (Fig. 2d) image modes of the bare alloy's surface before oxidation.

Besides, in the thicker oxide layer deposited after anodic oxidation, the deposition of phosphate particles from the oxidation solution is observed.

The oxide layer exhibits some fine porosity with diameters in the nanosize range (20 - 50 nm), favouring the reactions of ion exchange and electrostatic bonds with the ions and species from the human fluid, inducing the growth of the bone cells into pores and their strong adhesion.

3.4 Electrochemical and corrosion behaviour of oxide layer from polarisation measurements

Cyclic potentiodynamic polarisation curves from Fig. 3 indicated the self-passivation both of bare and anodic oxidation Ti-15Ta-5Zr alloys without active-passive region. The main electrochemical parameters (Table 1) revealed: more electropositive corrosion potentials, more

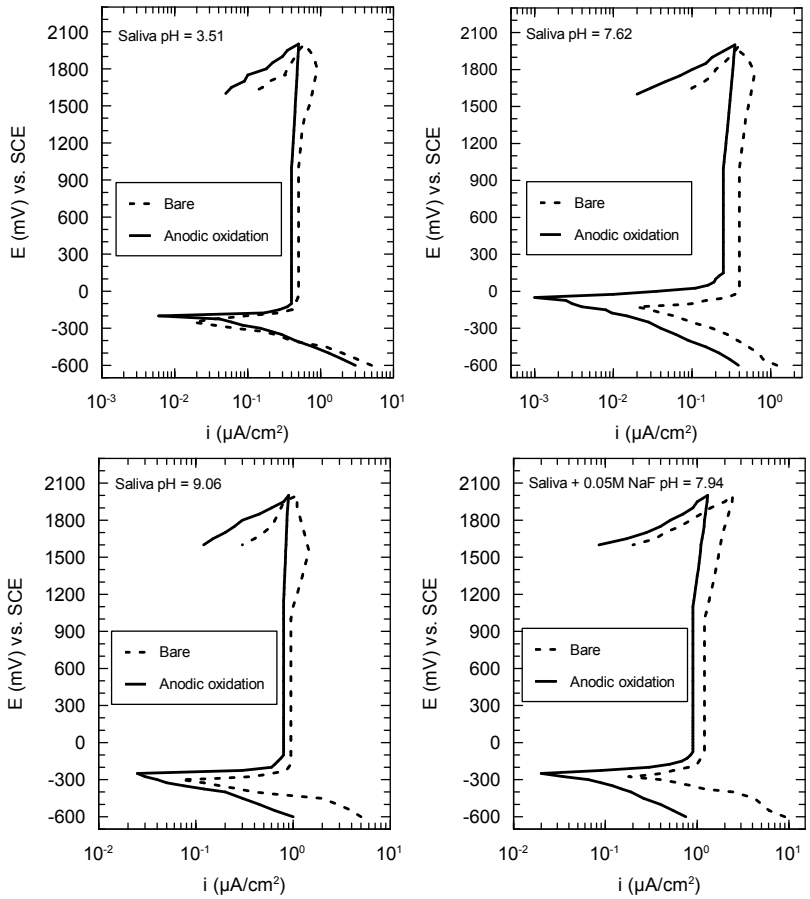

Fig. 3 Cyclic potentiodynamic polarisation curves for bare and anodic oxidation Ti-15Ta-5Zr alloy in Carter-Brugirard saliva of different pH values, at 37 °C.

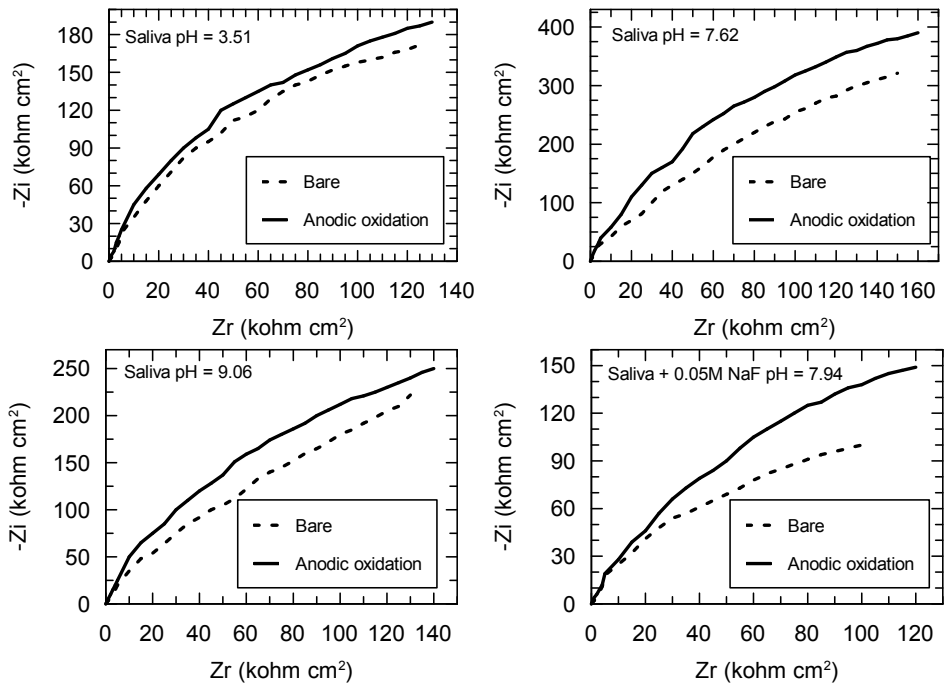

Fig. 4 Nyquist spectra for bare and anodic oxidation Ti-15Ta-5Zr alloy in Carter-Brugirard saliva of different pH values, at 37 °C.

Table 3 Parameters of the electric equivalent circuit for bare and anodic oxidation Ti-15Ta-5Zr alloy in Carter-Brugirard saliva, at 37 °C

Ti-15Ta-5Zr	R_{sol} (Ω cm^2)	R_1 (Ω cm^2)	CPE_1 (S s^n cm^{-2})	n1	R_2 (Ω cm^2)	CPE_2 (S s^n cm^{-2})	n2
Saliva of pH = 3.01							
Bare	15.6	3.1 x 10^6	3.3 x 10^{-6}	0.94	2.3 x 10^4	1.4 x 10^{-5}	0.89
Anodic oxidation	15.8	3.9 x 10^6	2.4 x 10^{-6}	0.96	2.6 x 10^4	1.1 x 10^{-5}	0.90
Saliva of pH = 7.22							
Bare	14.8	4.2 x 10^6	2.7 x 10^{-6}	0.96	4.4 x 10^4	1.2 x 10^{-5}	0.91
Anodic oxidation	14.9	5.5 x 10^6	1.2 x 10^{-6}	0.98	5.0 x 10^4	0.7 x 10^{-5}	0.94
Saliva of pH = 9.06							
Bare	15.8	3.3 x 10^6	3.1 x 10^{-6}	0.95	2.4 x 10^4	1.5 x 10^{-5}	0.90
Anodic oxidation	15.9	4.1 x 10^6	2.5 x 10^{-6}	0.96	2.8 x 10^4	1.2 x 10^{-5}	0.93
0.05M NaF Saliva pH = 7.94							
Bare	15.1	2.9 x 10^6	3.7 x 10^{-6}	0.93	2.1 x 10^4	1.7 x 10^{-5}	0.88
Anodic oxidation	12.4	3.5 x 10^6	3.2 x 10^{-6}	0.94	2.4 x 10^4	1.5 x 10^{-5}	0.90

Table 4 Open circuit potential gradients for bare and anodic oxidation Ti-15Ta-5Zr alloy in Carter-Brugirard saliva

Ti-15Ta-5Zr	Time (h)	ΔE_{oc1} (mV)	ΔE_{oc2} (mV)	ΔE_{oc3} (mV)	ΔE_{oc4} (mV)
Bare	0	-90	-50	+40	+110
	500	-35	-3	+32	+132
	1000	-20	-10	+30	+117
Anodic oxidation	0	-72	-28	+44	+122
	500	-30	-4	+31	+115
	1000	-25	+6	+31	+110

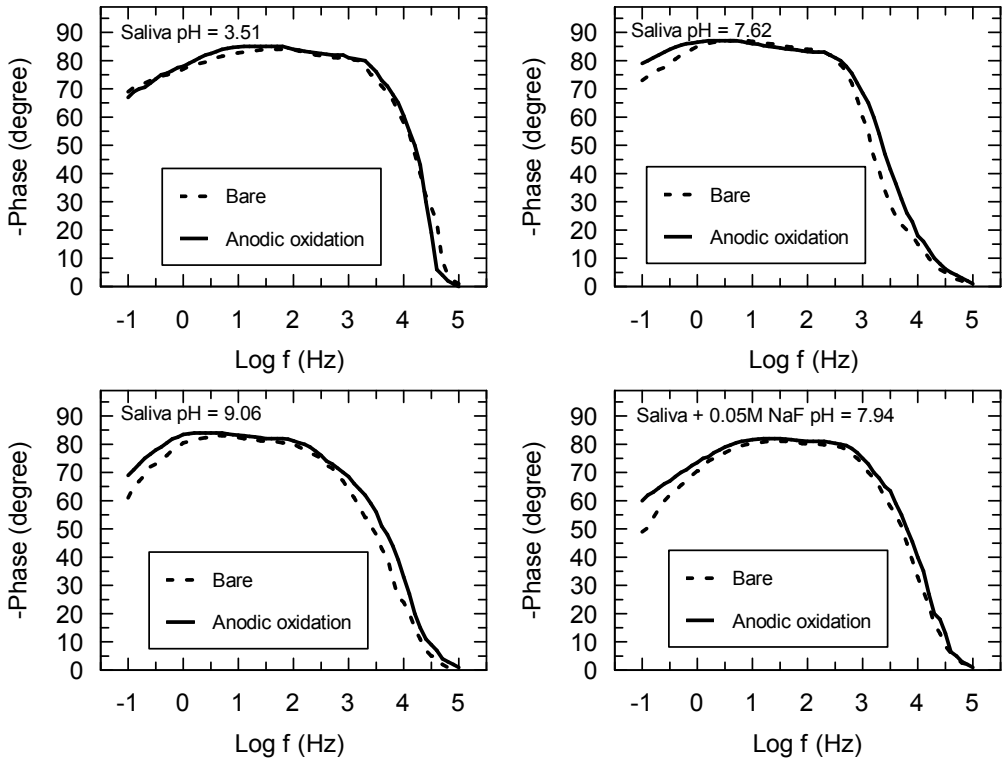

Fig. 5 Bode spectra for bare and anodic oxidation Ti-15Ta-5Zr alloy in Carter-Brugirard saliva of different pH values, at 37 °C.

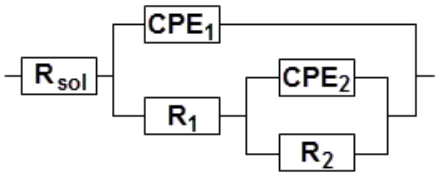

Fig. 6 Electric equivalent circuit.

electronegative passivation potentials, lower passive current densities for the processed alloy than those for the bare alloy; very good tendency to passivation and passive potential ranges > + 2000 mV. All these facts prove the beneficial effect of anodic oxidation that assures a homogeneous, thicker, more resistant oxide layer.

Main corrosion parameters from Table 2 show a better resistance to corrosion for anodic oxidation alloy: lower values of the corrosion current densities and corresponding corrosion rates and total quantity of ions released into the oral environment; higher values of polarisation resistance, which prove the improvement of the protective properties of the native oxide layer through anodic oxidation of new alloy's surface.

The acid and alkaline pH values of the artificial Carter-Brugirard saliva slightly negatively influenced the main electrochemical and corrosion parameters due to their increased aggressivity. The presence of the fluoride F^- ions in saliva, also conducted to the less favourable parameters.

3.5 Electrochemical and corrosion behaviour of oxidation layer from EIS measurements

The impedance Nyquist plots (Fig. 4) exhibited incomplete semicircles, demonstrating capacitive behaviour both for bare and oxidation alloy surfaces; the bigger diameters and impedance values for the protected alloy describe a more insulating, thicker, protective passive film on its surface [21].

Bode phase spectra (Fig. 5) displayed two phase angles; the higher phase angles had $-80^0 \div -84^0$ for bare alloy and $-83^0 \div -88^0$ for anodic oxidation alloy; the lower phase angles varied from $-78^0 \div -80^0$ for bare alloy and $-81^0 \div -84^0$ for oxidation alloy; the higher values of the phase angles for oxidation alloy prove a thicker, more stable oxide film on the new alloy surface after processing. Bode plots with two phase angles suggest an oxidation film with two layers: for the higher phase angle corresponds a barrier, inner layer and the lower phase angle indicates a porous, outer layer.

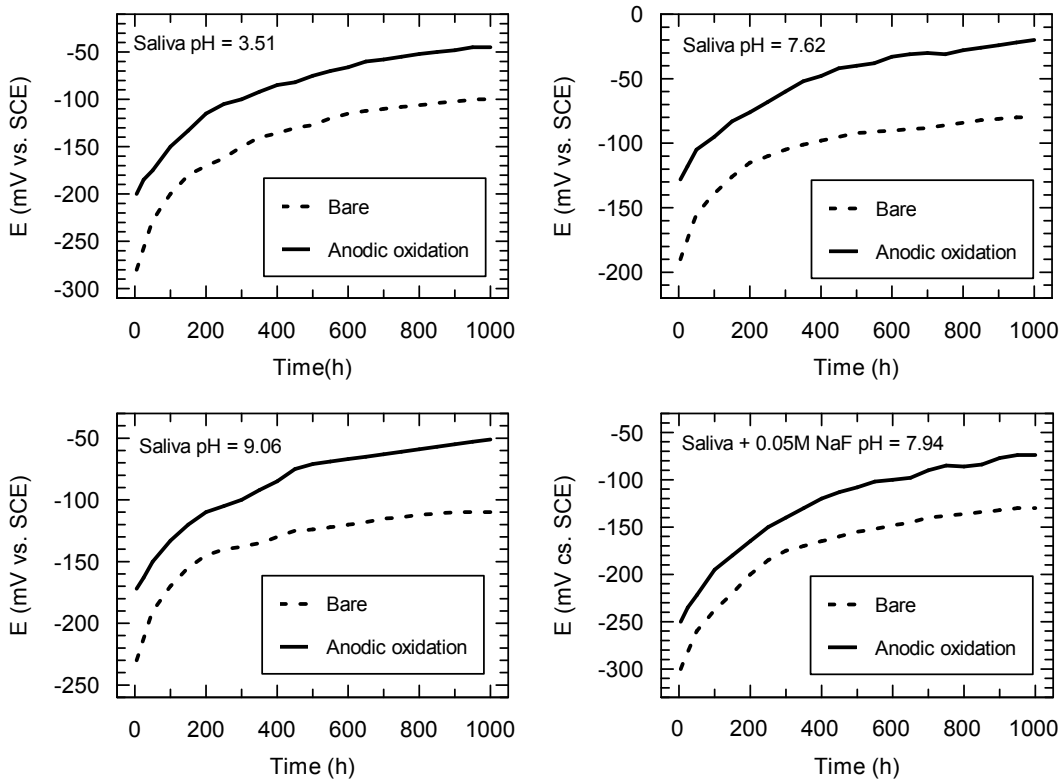

Fig. 7 Time monitoring of the open circuit potential for bare and anodic oxidation Ti-15Ta-5Zr alloy in Carter-Brugirard saliva of different pH values, at 37 °C.

The impedance results were fitted with an electric equivalent circuit comprising two time constants (Fig. 6): the first time constant is represented by resistance, R_1 and capacitance, CPE_1 of the barrier, inner layer; the second time constant is illustrated by the porous, outer layer (resistance, R_2 and capacitance, CPE_2).

The fitting parameters (Table 3) have more favourable values for the oxidation alloy, demonstrating the superior behaviour, higher resistance of the anodic oxide layer. The higher values of R_1 and n1 suggest an ideal capacitor; the lower values of the R_2 and n2 parameters indicate some interactions between the outer porous layer and the ions from the artificial saliva.

3.6 Monitoring of the open circuit potentials and corresponding open circuit potential gradients

Long-term monitoring of the open circuit potentials (1000 immersion hours) of the bare and anodic oxidization Ti-15Ta-5Zr alloy (Fig. 7) revealed a more accentuated shift to nobler values over time for the alloy with anodic oxidation surface; ennoblement of open circuit potentials is due to the thickening of the oxide film, which assures a superior behaviour in the physiological solutions. The noblest values of open circuit potentials were registered in neutral Carter-Brugirard saliva.

The open circuit potential gradients, ΔE_{oc}, which could appear along the implant surface in oral cavity due to the non-uniformities of the saliva pH and content have low values (Table 4) that cannot develop galvanic cells or local corrosion, because only potential differences of 600 – 700 mV can generate such corrosion types [22,23].

4. Conclusions

A layer of 15.5 nm thickness was electrodeposited using anodic oxidation, containing protective TiO_2, ZrO_2 and Ta suboxides and PO_4^{3-} ions incorporated from the phosphoric acid solution. The layer has very good roughness and porosity and favours the reactions of ion exchange and electrostatic bonds with the ions and species from the human fluid, inducing the growth of the bone cells into pores and their strong adhesion.

Main electrochemical parameters for the anodic oxidized alloy revealed a nobler behaviour, better stability due to its oxidation layer that thickened the initial, native passive layer, improving its protective properties.

The oxide layer enhanced all corrosion parameters assuring superior protection to the Ti-15Ta-5Zr alloy substrate by its higher resistance to the ion migration through it. For the oxidized alloy there is a significant decrease of the corrosion rates and total quantity of ions released into the oral environment compared to the bare one.

Impedance data revealed a bi-layered oxide film formed by: a compact, barrier layer in contact with the metallic substrate, capable to decrease the potential gradient across the metal/oxide layer/solution interface, so, reducing the anodic dissolution; a more permissive, porous layer in contact with the electrolyte for the activation of cell adhesion.

The open circuit potentials for the protected alloy shifted to nobler values, showing the thickening of the oxidation film, which means long-term protection and fewer adverse reactions. The dual character of the oxidation layer, barrier and porous, provides protection and bioactive abilities.

Acknowledgments

This work was supported by Romanian UEFSCDI, project no. TE 18/2013. Support of the EU (ERDF) and Romanian Government infrastructure POS-CCE o 2.2.1 project INFRANANOCHEM – No. 19/2009 is gratefully acknowledge. The authors are grateful to Dr. P. Osiceanu and Dr. M. Anastasescu from Institute of Physical Chemistry "Ilie Murgulescu" of Romanian Academy, Bucharest (Romania) for XPS and AFM analysis.

References

1. S. Guo, A. Chu, H. Wu, C. Cai, and X. Qu, *J. Alloy Compd.*, **597**, 211 (2014).
2. I. Cvijovic-Alagic, Z. Cvijovic, S. Mitrovic, V. Panic, and M. Rakin, *Corros. Sci.*, **53**, 796 (2011).
3. S. L. Assis and I. Costa, *Mater. Corros.*, **58**, 329 (2007).
4. A. Robin, O. A. S. Carvalho, S. G. Schneider, and S. Schneider, *Mater. Corros.*, **59**, 929 (2008).
5. M. Geetha, A. K. Singh, R. Asokamani, and A. K. Gogia, *Prog. Mater. Sci.*, **54**, 397 (2009).
6. D. M. Gordin, D. Busardo, A. Cimpean, C. Vasilescu, D. Höche, S. I. Drob, V. Mitran, M. Cornen, and T. Gloriant, *Mat. Sci. Eng. C*, **33**, 4173 (2013).
7. R. Palanivelu, S. Kalainathan, and A. Ruban Kumar, *Ceram. Int.*, **40**, 7745 (2014).
8. A. Nakahira, T. Kubo, and C. Numako, *ACS Appl. Mater. Inter.*, **2**, 2611 (2010).
9. R. Roest, B. A. Latella, G. Heness, and B. Ben-Nissan, *Surf. Coat. Technol.*, **205**, 3520 (2011).
10. R. B. Heimann, *Surf. Coat. Technol.*, **233**, 27 (2013).
11. C. Vasilescu, P. Drob, E. Vasilescu, I. Demetrescu, D. Ionita, M. Prodana, and S. I. Drob, *Corros. Sci.*, **53**, 992 (2011).
12. S. J. Li, R. Yang, M. Ninomi, Y. L. Hao, and Y. Y. Cui, *Biomaterials*, **25**, 2525 (2004).
13. C. Vasilescu, S. I. Drob, P. Osiceanu, M. Anastasescu, J. M. Calderon Moreno, P. Drob, and E. Vasilescu, *J.*

Nanomater., Volume 2014 Article ID 369034, p. 12 (2014).
14. V. W. Leung and B. W. Darvell, *J. Dent.*, **25**, 475 (1997).
15. R. Baboian, *Corrosion tests and standards: application and interpretation,* 2nd ed., pp. 1 - 882, ASTM International, West Conshohochen, Baltimore (2005).
16. R. Van Noort, *J. Mater. Sci.*, **22**, 3801 (1987).
17. J. M. Calderon Moreno, E. Vasilescu, P. Drob, P. Osiceanu, C. Vasilescu, S. I. Drob, and M. Popa, *Mater. Sci. Eng. B*, **178**, 1195 (2013).
18. E. Vasilescu, P. Drob, D. Raducanu, I. Cinca, D. Mareci, J. M. Calderon Moreno, M. Popa, C. Vasilescu, and J. C. Mirza Rosca, *Corros. Sci.*, **51**, 2885 (2009).
19. J. M. Calderon Moreno, M. Popa, S. Ivanescu, C. Vasilescu, S. I. Drob, E. I. Neacsu, and M. V. Popa, *Met. Mater. Int.*, **20**, 177 (2014).
20. C. Vasilescu, S. I. Drob, J. M. Calderon Moreno, P. Osiceanu, M. Popa, E. Vasilescu, M. Marcu, P. Drob, *Corros. Sci.*, **93**, 310 (2015).
21. M. T. Woldemedhin, D. Raabe, and A. W. Hassel, *Electrochim. Acta*, **82**, 324 (2012).
22. C. Sola, A. Amorim, A. Espias, S. Capelo, J. Fernandes, L. Proenca, L. Sanchez, and I. Fonseca, *Int. J. Electrochem. Sci.*, **8**, 406 (2013).
23. G. Sheela, M. Ramasamy, C. R. K. Rao, and M. Pushpavanam, *Bull. Electrochem.*, **17**, 347 (2001).